# JMB

AP

# Torque–speed Relationship of the Na+-driven Flagellar Motor of *Vibrio alginolyticus*

## Yoshiyuki Sowa[1], Hiroyuki Hotta[2], Michio Homma[3] and Akihiko Ishijima[2,4]*

[1]*Department of Biophysical Engineering, Osaka University 1-3, Machikaneyama, Toyonaka Osaka 560-8531, Japan*

[2]*Department of Applied Physics Graduate School of Engineering Nagoya University Furo-cho, Chikusa-ku Nagoya, Aichi 464-8603, Japan*

[3]*Division of Biological Science Graduate School of Science Nagoya University Furo-cho, Chikusa-ku Nagoya, Aichi 464-8602, Japan*

[4]*PRESTO, Japan Science and Technology Corporation (JST), Japan*

*Corresponding author

The torque–speed relationship of the Na+-driven flagellar motor of *Vibrio alginolyticus* was investigated. The rotation rate of the motor was measured by following the position of a bead, attached to a flagellar filament, using optical nanometry. In the presence of 50 mM NaCl, the generated torque was relatively constant ($\sim$3800 pN nm) at lower speeds (speeds up to $\sim$300 Hz) and then decreased steeply, similar to the H+-driven flagellar motor of *Escherichia coli*. When the external NaCl concentration was varied, the generated torque of the flagellar motor was changed over a wide range of speeds. This result could be reproduced using a simple kinetic model, which takes into consideration the association and dissociation of Na+ onto the motor. These results imply that for a complete understanding of the mechanism of flagellar rotation it is essential to consider both the electrochemical gradient and the absolute concentration of the coupling ion.

## Introduction

The bacterial flagellar motor is a rotary molecular machine powered by the flow of ions across the cytoplasmic membrane.[1] Each motor rotates a long ($\sim$5 μm) helical filament that extends from a cell body. The rotation of this filament is used for cell propulsion, which is the primary method of locomotion. The influx of ions is driven by a transmembrane electrochemical gradient of a specific ion, either H+ (protonmotive force: pmf) or Na+ (sodium-motive force: smf).[2–4] H+-driven type flagellar motors are used in *Bacillus subtilis*, Streptococcus or *Escherichia coli*, and Na+-driven type flagellar motors are found in alkalophilic Bacillus or Vibrio species.

In H+-driven flagellar motors, approximately 50 proteins are required for the assembly and rotation of the flagella.[5] Especially, MotA, MotB and FliG are essential for the conversion of energy to torque

and have been identified from genetic studies of *Salmonella typhimurium* and *E. coli*.[6,7] MotA and MotB form a proton channel complex and function as a component of a stator.[6] The rotor consists of a series of rings spanning the cell envelope, which is attached *via* the flexible hook to the helical filament,[8] and is surrounded by eight or 16 independent MotA/B complexes.[9,10] FliG forms part of the rotor and interacts with MotA to generate torque for rotation. Analyses of site-directed mutagenesis have shown that the charged residues crucial for torque generation are R90 and E98 in MotA and R281, E288 and E289 in FliG.[11,12] It is thought that these charged residues of MotA and FliG engage in electrostatic interactions with each other. When either R90 or E98 of MotA was converted to Glu or Lys, the motor was unable to rotate.[13]

PomA and PomB in Na+-driven flagellar motors have sequences similar to MotA and MotB in the H+-driven motors, respectively, and function as sodium channels. PomA in *V. alginolyticus* conserves charged residues such as R88 and E96, which correspond to R90 and E98 of MotA of *E. coli*, respectively. In contrast to the H+-driven
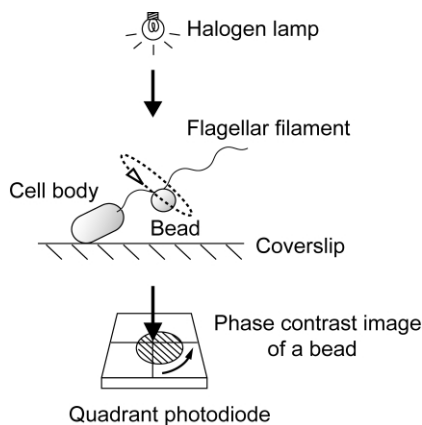
**Figure 1**. Schematic of a measurement system of Na$^+$-driven flagellar motor rotation in NMB136 cells. An NMB cell was immobilized on the glass surface and a bead was attached to its flagellar filament. The phase-contrast image of the bead was projected onto the face of a quadrant-type photodiode (see the text for details).

motor, reversal of the charge of either R88 or E96 had no effect on flagellar rotation of the Na$^+$-driven motors.[14] Torque generation of Na$^+$-driven motors requires the additional components MotX and MotY.[15,16] The components of the H$^+$-driven flagellar motor had no similarities with MotX and MotY, except for the fact that the C terminus of MotY has a peptidoglycan-binding motif.[17] MotX and MotY are located in the outer membrane[18] and interact with each other.[19] MotX and MotY appear to be components unique to the Na$^+$-driven flagellar motors; however, their precise roles have not been determined. Although there are differences between H$^+$-driven and Na$^+$-driven motors, it is thought that both motors operate by the same underlying mechanism because PomA defective *V. alginolyticus* cells can regain flagellar rotation by expressing MotA of *Rhodobacter sphaeroides*, which has a H$^+$-driven motor.[20]

Many models explaining the mechanism of the bacterial flagellar rotation have been proposed.[21,22] To verify these models, the function of the rotary motor must be investigated. The most common method for investigating flagellar rotation has been the tethered cell method.[23] This method involves attaching a single flagellar filament to a microscope coverslip using antibodies against the filament and observing the rotation of the cell body. This is a very convenient method from the view-point that no specialized equipment is necessary. However, the motor operates at approximately 10 Hz due to the unnatural high loads imposed on the motor. Normal flagella rotate at speeds greater than 100 Hz.[24] In an extension of the tethered cell method, the method of electrorotation has been applied to study flagellar motors.[25] This method controlled the rotation rates of cells by applying an external torque and clarified the torque–speed relationship of *E. coli*.[26] Another effective method of measuring flagellar rotation

involves laser dark-field microscopy.[27] In this method, a thin laser beam irradiates the flagellar filament and the rotation rate under natural load conditions can be measured from the intensity change of the scattered light with high temporal resolution. The average rotation rate using this method is reasonably stable; however, there are abrupt slowdowns, pauses and reversals of the rotation.

A method used to measure the displacement of biological molecules with high temporal and spatial resolutions has been developed recently. This method involves attaching a bead as a marker to molecules and projecting the bead image onto a photo-detector.[28] This method has greatly advanced the studies of motor proteins that perform sliding movements, such as kinesin and myosin.[29–31] This bead assay has also been applied to studies of the flagellar motors. A spherical bead was attached to the flagellum or hook and the position of the bead was followed by photo-detector.[32] Careful experiments using a bead assay confirmed the torque–speed relationship of the H$^+$-driven flagellar motor in *E. coli*.[32,33]

In this study, the flagellar rotation of the Na$^+$-driven motor in *V. alginolyticus* was measured using a bead assay. The torque–speed relationship of the Na$^+$-driven flagellar motor is similar to that of the H$^+$-driven flagellar motor. This result suggests that the mechanism of torque generation in both Na$^+$ and H$^+$-driven is similar. A kinetic model applied to the data could reproduce the effect of NaCl concentration in the medium on the generated torque.

## Results

### Measurement of flagellar rotation using a bead assay

The rotation rates of Na$^+$-driven flagellar motors in *V. alginolyticus* NMB136 have been measured by attaching a poly-L-lysine modified bead to a flagellar filament as a marker (Figure 1). NMB136 cells are useful for measurements of flagellar rotation, because (1) these cells have a single polar flagellar motor, no lateral flagella (Laf$^-$), and (2) a flagellum rotates unidirectionally, i.e. without the clockwise direction (Che$^-$).[34] The polar flagellar filament of *V. alginolyticus* is sheathed, and the components of the sheath are thought to be similar to that of the outer membrane.[35] Because beads have not been rarely observed attached to the cell body under our experimental conditions and the membrane enclosing the filament is supposed to be too fragile to rotate with the beads, it is likely that the poly-L-lysine modified beads attached to exposed areas on the filaments. To follow the position of the beads with sub-millisecond and nanometer resolution, a phase-contrast image of the bead was projected onto the face of a quadrant-type photodiode.[36] Currents from each of the
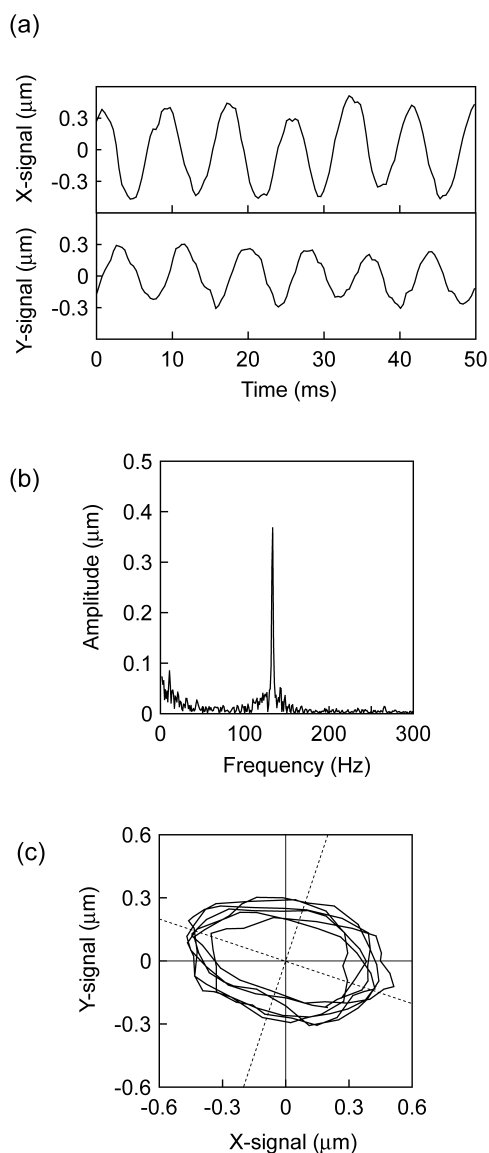
(a)



(b)



(c)



**Figure 2**. Typical example of the data. (a) $X$ and $Y$ signals of the position of a bead attached to the flagellar filament are shown as a function of time. The size of the bead was 1.08 μm in diameter. The external NaCl concentration was 50 mM. The signals were passed through a low-pass filter of 1 kHz. (b) The FFT spectrum of the signal from 1.0 second using the same data as in (a). (c) A two-dimensional $X-Y$ plot of the data shown in (a). Broken lines are the major and minor axes of the ellipsoid.

(a)



(b)



**Figure 3**. (a) The effect of NaCl concentration on the swimming speed of *V. alginolyticus* NMB136 cells. Each point shows the average swimming speed for 50 cells measured in several independent experiments in the presence of varying NaCl concentrations. The $Y$-axis on the right represents the flagellar rotation rate calculated from the $v:f$ ratio.[37] (b) The relationship between the concentration of NaCl in the external medium and the rotation rate of beads attached to the flagellar filaments. Crosses ( × ), filled diamonds (◆) and open circles (○) show the average values of rotation rate when beads of 1.08, 0.85 and 0.60 μm diameter were attached to flagellar filaments, respectively. For each data point, at least eight cells were measured.

four quadrants were converted to voltages, and the $X$ signal and $Y$ signal of the bead position were calculated through a differential amplifier. Figure 2(a) shows the typical time-course of the $X$ and $Y$ signals of the bead position when a bead 1.08 μm in diameter was attached to a flagellar filament. Since the bead was rotating, the $X$ and $Y$ signals appeared as sinusoidal curves with a 90° phase shift. The FFT spectrum in the $X$ signal (or $Y$ signal) had a single peak, and its frequency was 133 Hz, so this has been taken as the rotation rate of the flagellar motor (Figure 2(b)). The experimental
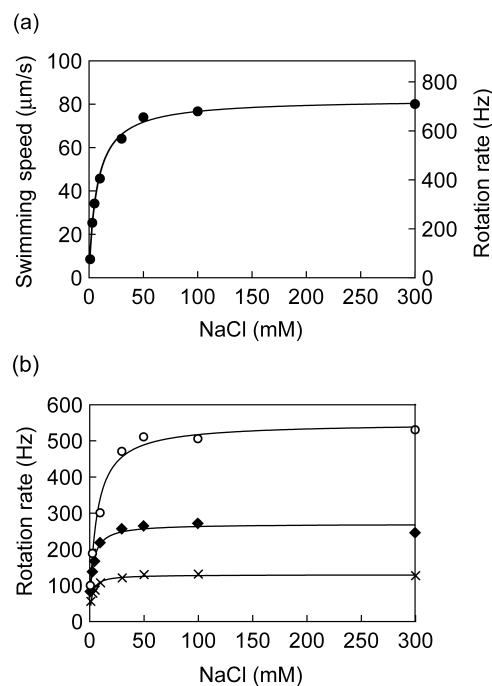
conditions in this measurement system, such as light intensity, had little effect on the flagellar rotation. Most cells rotated their flagellar filaments at a constant speed for at least ten minutes.

Cells that tilted up from the surface of a coverslip (as illustrated in Figure 1) were selected, because this orientation allowed us to ignore the friction between the beads and the coverslips. This resulted in the two-dimensional $X-Y$ plots of most of the acquired data being ellipsoid in shape. Then, the rotational radii of the beads were measured as the major radius of the ellipsoid. Figure 2(c) shows the $X-Y$ plot of the bead positions of a bead 1.08 μm in diameter. The rotational radius of the bead was measured as 0.43 μm. This value is reasonable, because the rotational radius is expected to be $r_b \pm r$, where $r_b$ is the radius of a bead and $r$ is the helical radius of the flagellar filament, 0.14 μm.[37] However, the rotational radii of beads were often larger than expected. This was especially so for beads with diameters of 1.65 μm and 1.08 μm, and is most likely due to the eccentric rotation of the flagellar filaments.

## The effect of external NaCl concentrations on flagellar rotation

Figure 3(a) shows the effect of external NaCl concentration on the swimming speed of NMB136 cells. NMB136 cells have a single polar flagellar motor, so the swimming speed should reflect the rate at which the flagellum rotates. Studies using laser dark-field microscopy reported that external concentration of NaCl affected the swimming speed and the flagellar rotation rate.[38] The swimming speed and the flagellar rotation rate were measured simultaneously in *V. alginolyticus*.[37] The relation between swimming speed ($v$) and flagellar rotation ($f$) can be defined by the equation:

$$v \, (\mu m/s) = 0.113 \, (\mu m) \times f \, (1/s)$$

The flagellar rotation rate expected using the $v$:$f$ ratio is described in the $Y$-axis on the right of Figure 3(a).

The flagellar rotation rates were measured using a bead assay in the presence of different concentrations of NaCl (Figure 3(b)). As the swimming speed, the rotation rate of the bead attached to the flagellar filament increased with the external NaCl concentrations and reached a maximum speed at a NaCl concentration of approximately 100 mM. The profile was basically the same for all beads used. The rotation rates at any NaCl concentration decreased with an increase in the bead size. For example, at high NaCl concentrations, the saturated or maximal rotation rates of beads 0.60 μm, 0.85 μm and 1.08 μm in diameter attached to the flagellar filament were 500 Hz, 250 Hz and 130 Hz, respectively. This indicates that beads exerted the load on the motor. These results suggest that in our measurement system, the rotation of the bead reflects flagellar rotation under various load conditions and that attaching a bead does not cause any effects except loads to flagellar rotation.

## The torque−speed relationship of Na+-driven flagellar motors

In this study it was possible to estimate the generated torque of the Na+-driven flagellar motor. The generated torque of the motor ($M$) was calculated from the rotational frictional drag coefficient ($f_r$) multiplied by the angular velocity ($\omega$), $M = f_r \times \omega$.[39] The rotational frictional drag coefficient was estimated from the sum of that resulting from the rotation of a bead ($f_b$) and a flagellar filament ($f_f$) (for more details see Materials and Methods). To study the generated torque over a wide range of speeds, the $f_r$ value was changed from 0.5 pN nm s to 20 pN nm s by using beads of different sizes (0.46−1.65 μm in diameter).

Figure 4(a) shows the torque−speed relationship of Na+-driven flagellar motors at a NaCl concentration of 50 mM. Each point, except the open diamond, represents a value of the generated torque measured from one cell. The symbols represent torque values from beads attached to the
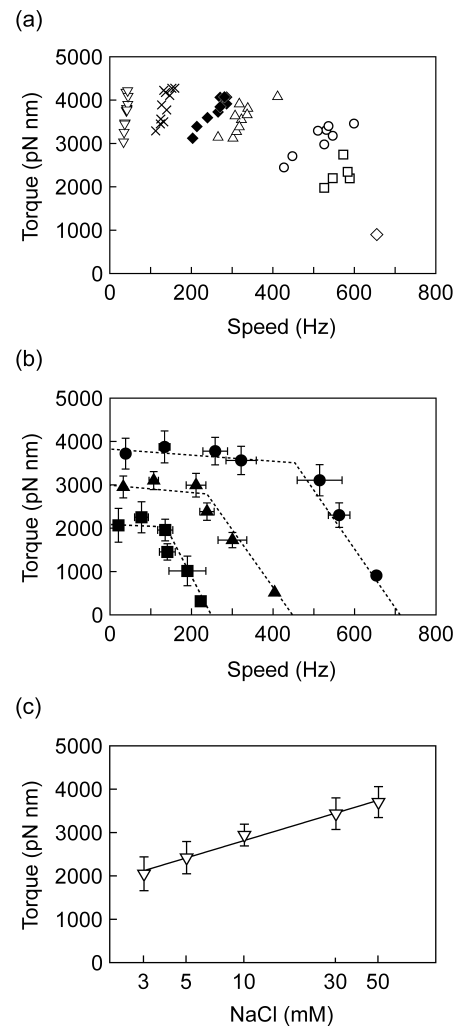


**Figure 4.** (a) Torque−speed relationship at a NaCl concentration of 50 mM. Symbols represent the bead sizes as follows: ▽, 1.65 μm; ×, 1.08 μm; ◆, 0.85 μm; △, 0.75 μm; ○, 0.60 μm; □, 0.46 μm; and ◇, no bead attached. (b) The effect of NaCl concentration on the torque−speed relationship. Symbols and error bars indicate the average values and standard deviation for each size of a bead, respectively. Circles (●), triangles (▲) and squares (■) are derived from experiments at NaCl concentrations of 50, 10 and 3 mM, respectively. At the concentrations of 10 and 3 mM NaCl, a bead 0.46 μm in diameter was not used. (c) The relationship between the generated torque and NaCl concentration when a bead 1.65 μm in diameter was attached to the flagellar filament. The horizontal scale is logarithmic.

flagellar filament having diameters of 1.65, 1.08, 0.85, 0.75, 0.60 and 0.46 μm. The open diamond plotted in Figure 4(a) was the generated torque without a bead attached to the filament and was calculated by using data of the rotation rates of flagellar filaments (Figure 3(a)). The torque generated between 0 Hz and 300 Hz was relatively constant at 3800 pN nm. In the high-speed region, the generated torque declined steeply. The torque−speed relationship of Na+-driven flagellar motors in *V. alginolyticus* is similar to that of H+-driven

motors in *E. coli*, although the flagellar rotation in *V. alginolyticus* is considerably faster than in *E. coli*.[33] Next, the torque–speed relationship was measured at NaCl concentrations of 3, 10 and 50 mM (Figure 4(b)). These curves show similar trends in the presence of any concentrations of NaCl; that is, the generated torque was constant at low speeds and decreased in the high-speed region. However, both torque and speed decreased with decreasing external NaCl concentrations. The maximum torque, stall torque, is approximately 3800, 3000 and 2100 pN nm at NaCl concentrations of 50, 10 and 3 mM, respectively. The zero-torque speed estimated by extrapolating the values in the high-speed region was 710, 450 and 250 Hz in the presence of 50, 10 and 3 mM NaCl, respectively. The effect of the concentration of NaCl on the flagellar motor seems to be greater in the high-speed region. Figure 4(c) shows the relationship between the generated torque and the external NaCl concentrations when a bead 1.65 μm in diameter was attached to a flagellar filament. In this condition, the load exerted on the motor is very high, like that of the tethered cell. The torque generated by Na⁺-driven flagellar motors under high load conditions is a linear function of the logarithm of NaCl concentrations between 3 and 50 mM.

## Discussion

Many models of the rotational mechanism of the bacterial flagellar motor have been proposed to explain the relationship between the input and output of the motor.[40–45] The input of the flagellar motor is considered to be the ion-motive force and the ion fluxes, and the output of the motor is characterized by its torque and rotation rate. In order to understand the mechanism of the motor, it is essential to know the relationship between the input and output in detail. Here, the rotation rate and the generated torque as outputs of the Na⁺-driven flagellar motor of *V. alginolyticus* were measured using a bead assay and the results obtained were compared to a simple kinetic model. Na⁺-driven motors are useful for modulating inputs of the motor as the rotation rate can be altered by changing the external NaCl concentration. A bead assay is a very effective method for detecting the rotation rates of flagellar motors using a conventional optical microscope equipped with a quadrant-type photodiode. The spherical bead is attached to a flagellar filament as a marker. In our system, beads larger than 0.46 μm in diameter produced sufficient signal intensity to follow the position of the bead. This assay will also allow the switching mechanism of the flagellar motor to be investigated, since it measures not only the rotation rate but also the rotational direction.

The torque generated by the motor with a bead attached can be determined by the angular velocity

of the motor times the viscous drag which can be calculated as the sum of the flagellar filament and the bead. The torque–speed relationship of the Na⁺-driven flagellar motor was estimated by changing the viscous drag on the motor, i.e. using beads of different sizes. At a NaCl concentration of 50 mM, the torque was relatively constant at 3800 pN nm at low speed (speeds up to ∼300 Hz). This value corresponds to the maximum torque values obtained for *E. coli*, (6300 pN nm[46] or 4500 pN nm[47]), and for *Streptococcus* (3000 pN nm[24]). In the high-speed region, the generated torque decreased steeply. This pattern observed in the torque–speed curve of *V. alginolyticus* was similar to that shown in *E. coli*.[26,33] These results suggest that the mechanism of torque generation in Na⁺-driven flagellar motors is similar to that in H⁺-driven motors, although the charged residues essential for the interaction between the stator and rotor seem to be different.[13,14]

It is thought that the bacterial flagellar motor is rotated by the sum of the torque generated by independently functioning force-generating units in both H⁺ and Na⁺-driven motors.[9,10,48] The number of force-generating units of Na⁺-driven flagellar motors was estimated to be five to nine units in alkalophilic *Bacillus* using a photoreactive inhibitor of a sodium channel[48] and five to eight units in *V. alginolyticus* using the same reagent (our unpublished results). From the experimental results (3000 pN nm at 500 Hz in the presence of 50 mM NaCl; Figure 4(b)), the maximum power of each unit can be estimated to be at least $1.0 \times 10^6$ pN nm s⁻¹ even when eight units are involved in torque generation, where the output of the power is defined as torque multiplied by the angular velocity. This value is larger than that obtained in *E. coli*, $1.75 \times 10^5$ pN nm s⁻¹.[32]

When external NaCl concentrations were changed, the torque–speed relationships in the presence of any NaCl concentration showed similar trends (the torque was constant in the low speed region and declined steeply in the high speed region). The NaCl concentration had a great influence on the values of the torque and rotation rate obtained in the torque–speed curve (Figure 4(b)). The effect of the concentrations of the coupling ion on torque–speed curves of *V. alginolyticus* was different from those of *E. coli*. The curves for *E. coli* did not change even when the external environment had a pH value in the range pH 4.7–8.8.[49] The difference in the effect of the coupling ion on the torque–speed relationship between *V. alginolyticus* and *E. coli* is possibly derived from the difference not in the mechanism of flagellar motors but in the cell homeostasis when the concentration of the external coupling ion is varied. In *E. coli* when the external pH is varied the cells can maintain the cytoplasmic pH value, but the pmfs do not change considerably by adjusting their membrane potential.[50] In the cells that have Na⁺-driven motors, the membrane potential of the

cells, $\Delta\Psi$ is almost independent of the external Na$^+$ concentration.[51,52] However, there are conflicting reports on whether the cytoplasmic Na$^+$ concentration of cells increases linearly with the external Na$^+$ concentration[52] or remains constant at 30 mM.[51] The exact effect that the external concentrations of NaCl have on the cytoplasmic Na$^+$ concentration is unknown. However, the effect of the external NaCl concentration on the cytoplasmic Na$^+$ concentration could be predicted. Using tethered cells of Streptococcus under high load conditions, the generated torque of the flagellar motor was a linear function of the pmf.[53] We applied this result to the Na$^+$-driven motors in our system; that is, the generated torque was applied as a linear function of:

$$\text{smf} = \Delta\Psi - 59 \log[\text{Na}^+]_{\text{out}}/[\text{Na}^+]_{\text{in}}$$

where $[\text{Na}^+]_{\text{out}}$ and $[\text{Na}^+]_{\text{in}}$ are the external and cytoplasmic Na$^+$ concentrations, respectively. At high loads the generated torque was a linear function of the logarithm of the NaCl concentration (Figure 4(c)). Therefore, it is likely that the cytoplasmic Na$^+$ concentrations remain stable even when the external NaCl concentrations vary.

These experimental results were then simulated using a simple kinetic model in an attempt to demonstrate the effect of Na$^+$ concentration on the torque–speed curve.[44,46] The Na$^+$-driven flagellar motor was reported to have both external and cytoplasmic Na$^+$ binding sites.[54] Figure 4(b) shows that the effect of the concentration of NaCl on the flagellar motor is greater in the high-speed region. These results suggest that the association and dissociation of Na$^+$ on the binding sites limit the kinetic cycle. Thus, the four-state model proposed by Iwazawa et al.[46] was adopted with some modifications. This model takes into consideration the external and cytoplasmic concentrations of Na$^+$ (Figure 5(a)). As in the study by Iwazawa et al.,[46] we have also assumed the four-state model as follows. (1) Each force-generating unit of the motor has binding sites for Na$^+$ on both sides of the membrane. (2) Binding sites are non-charged carriers and move both in backward and forward directions with a transmembrane rate constant, $k_0$. (3) Charged carriers move with a rate constant, $k_A$ or $k_B$, and participate in torque generation. When $\text{M}_\text{o}\cdot\text{Na}^+$ is transformed to $\text{M}_\text{i}\cdot\text{Na}^+$ with a rate constant $k_A$, an external sodium ion is transported into the cytoplasm. Consequently the rotor rotates with a given angle, $\phi$, and generates torque. (4) As for all reactions a reverse reaction can occur.

In this simulation, the step angle, $\phi$, was assumed to be fixed under any condition. When the rotor rotates one revolution, the influx of Na$^+$ through the multiple force generating units ($n_\text{u} = 8$ units) can be defined as $2\pi n_\text{u}/\phi$. In this study, the net flux was taken to be 1000 ions per revolution, the value measured for Streptococcus.[55] Figure 5(b) shows the result of the simulation using the values described above, when $[\text{Na}^+]_{\text{in}}$ and $\Delta\Psi$
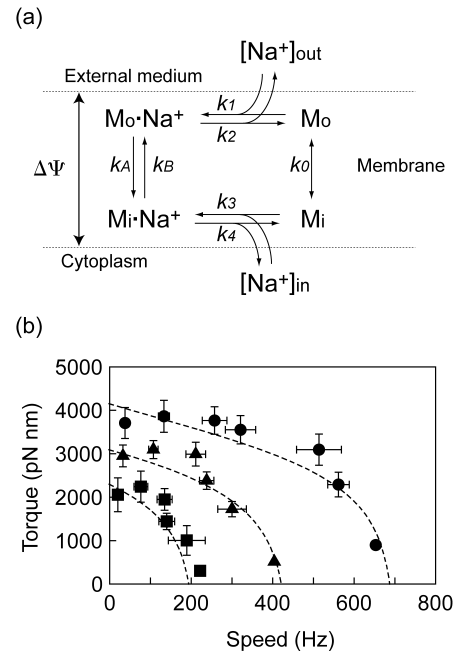


**Figure 5**. (a) A kinetic model for the cyclic reaction in the bacterial flagellar motor. When a Na$^+$ in the external medium flows into the cytoplasmic medium, the procedure is as follows. (i) A Na$^+$ in the external medium binds to site $\text{M}_\text{o}$, which faces the external medium, with the rate constant, $k_1$, and forms $\text{M}_\text{o}\cdot\text{Na}^+$; (ii) the charged carrier, $\text{M}_\text{o}\cdot\text{Na}^+$, moves across the membrane with the rate constant, $k_A$, and transforms into $\text{M}_\text{i}\cdot\text{Na}^+$; (iii) $\text{M}_\text{i}\cdot\text{Na}^+$ releases Na$^+$ with the rate constant, $k_4$, and to form $\text{M}_\text{i}$; (iv) $\text{M}_\text{i}$ returns to the initial state $\text{M}_\text{o}$ with the rate constant, $k_0$. As for all reactions, a reverse reaction may also occur. The transition across the cytoplasmic membrane of a non-charged carrier is determined by the absolute rate constant, $k_0$. The transition rate constants of charged carriers, $k_A$ and $k_B$, are given by $k_A = k_0 \exp\{-(M\phi/n_\text{u} + e\Delta\Psi)/2kT\}$ and $k_B = k_0 \exp\{(M\phi/n_\text{u} + e\Delta\Psi)/2kT\}$, respectively, where $k$ is the Boltzmann constant, $e$ is the charge of an ion, $T$ is the absolute temperature, $M$ is the generated torque, $n_\text{u}$ is the number of torque generators, $\Delta\Psi$ is the membrane potential and $\phi$ is the angle moved in one cycle. In this simulation, it has been assumed that the kinetic cycle is in a steady-state. Steady-state occupancy probabilities ($[\text{M}_\text{o}]$, $[\text{M}_\text{i}]$, $[\text{M}_\text{o}\cdot\text{Na}^+]$, $[\text{M}_\text{i}\cdot\text{Na}^+]$) were calculated from four equations assuming that the time change to each state is zero. The net rate of the mechano-chemical cycle ($k_C$) is given by $k_C = k_A[\text{M}_\text{o}\cdot\text{Na}^+] - k_B[\text{M}_\text{i}\cdot\text{Na}^+]$, and the rotation rate of the flagellar motor is calculated from $k_C\phi/2\pi$. See the text, Iwazawa et al.[46] and Berry & Berg[44] for details. (b) Simulation of the dependence of the external NaCl concentration on the torque–speed relationship. Symbols are the same as used for Figure 4(b). Parameters used to reproduce the experimental results are as follows; $k_0 = 5.0 \times 10^5 \text{ s}^{-1}$, $k_1 = k_3 = 6.0 \times 10^7 \text{ M}^{-1} \text{ s}^{-1}$ and $k_2 = k_4 = 6.0 \times 10^5 \text{ s}^{-1}$.

are 30 mM and −150 mV, respectively. This model can explain the essential features of the effect of NaCl concentration on the torque–speed relationship using the appropriate parameters of the rate constants. Since the values of all rate constants in this simulation, translation, association and

dissociation of $Na^+$, are in a similar range, it is likely that all kinetic steps could be rate limiting in this cycle. In other words, the steps of the association and dissociation of the coupling ions are essential processes. The simplified model that considered smf as an input could not reproduce the effect of the external $Na^+$ concentration on the torque–speed relationship in our results, because this model predicts that the external $Na^+$ concentration seldom had an affect in the high-speed region. Thus, it is necessary not only to consider the simple gradients but also the absolute concentration of the coupling ion when the models of the flagellar rotation are proposed, as predicted by Yoshida *et al.*[54] and Minamino *et al.*[56] However, in the high-speed region, although the generated torque decreased steeply in our experimental results, a vertical slope in the torque–speed curve was observed in the four-state model. Results from electrorotation studies show that the larger rotation rates were observed when the larger torque was applied to the flagellar motor in a counter-clockwise direction.[26] In our simulations, even when an external force is applied to the flagellar motor, forcing it to rotate in a counter-clockwise direction, the rotation rate does not increase more than the zero-torque speed. Two possibilities can explain this problem. One is that all steps in the four-state model depend on the term of the generated torque, as shown by Berry & Berg.[44] The slope of torque–speed curve in the high-speed region is more sensitive to the weak torque-dependent transitions. In the four-state model, if all transitions contribute to torque generation, the change in slope of the generated torque will be shallower in the high-speed region. The second possibility is that the angle moved in one cycle, ϕ, should be changeable according to the generated torque. If the step angle, ϕ, generated in the high-speed region is larger than in the low-speed one, as observed in muscle contraction,[57] then the torque–speed curve obtained here and in the study of electrorotation could also be explained by the four-state kinetic model. Thus, it is very important when considering the mechanism of the flagellar motor rotation to determine the rotational angle of the single processes and the effect of the load being exerted on the motor. From now on, we will need to develop a measurement system with high enough sensitivity to detect such fine movements.

## Materials and Methods

### Bacterial strains and the experimental media

A smooth-swimming mutant of *V. alginolyticus*, strain NMB136, was used in this study.[34] Cells were cultured to the late logarithmic phase at 30 °C in VPG medium (1% (w/v) polypeptone, 0.4% (w/v) $K_2HPO_4$, 3% (w/v) NaCl, 0.5% (w/v) glycerol). The swimming speed and the flagellar rotation rates of the cells were measured in TMN medium (50 mM Tris–HCl (pH 7.5), 5 mM $MgCl_2$,

5 mM glucose, 300 mM NaCl + KCl). Measurements were performed after the cells were suspended in the TMN medium with the appropriate experimental NaCl concentration for at least 30 minutes.

### Preparation of poly-L-lysine modified beads and immobilization of cells

Carboxylated beads were incubated in 5 mg/ml poly-L-lysine (P-7890; Sigma Chemical Co.) in 0.4 M KOH solution on ice for three hours. The beads were centrifuged and washed repeatedly in TMN medium (0 mM NaCl) and stored on ice. The rotational frictional drag coefficient of the motor was changed by using beads of different sizes. Beads with diameters of, 1.65, 1.08, 0.75 (Polysciences), 0.85, 0.60 (Bangs Laboratories) and 0.46 μm (Molecular Probes) were used. The cell suspension was mixed with diluted poly-L-lysine modified beads and introduced into the flow cell. To detect flagellar rotation, cells, which had a single bead attached to the filament and were immobilized to the surface of a cleaned coverslip, were selected.

### Measurement of flagellar rotation

An inverted microscope (IX70; Olympus, Japan) with a phase-contrast objective (UplanApo ×60, NA 1.4; Olympus, Japan) was used for following flagellar rotation. The microscope was placed on an air-damping table (TDIS-189LA; Herz, Japan). The microscope specimen could be moved by between ∼1 nm and 10 mm using a hydraulic micromanipulator (MHW-103; Narishige, Japan) with a handmade piezo-electric stage moved by piezo stacks (AE0203D08; TOKIN, Japan). The phase-contrast image of the bead, which was attached to a flagellar filament, was projected onto the face of a quadrant-type photodiode (S-6242; Hamamatsu Photonics, Japan), which was placed in the image plane of the camera port of the microscope, coupled to a differential amplifier (OP711; Sentec, Japan). The bead positions were recorded at a sampling rate of 48 kHz by a DAT recorder (RD-125T; TEAC, Japan), and analysed offline by using DADiSP software (DSP Development Corp.). The acquired data were passed through a digital recursive Chebyshev type 1 low-pass filter of adequate bandwidth according to the rotation rate of a bead. The rotation rate of a motor was computed from a peak in the FFT spectrum of a bead position ($X$ or $Y$ channel), and the rotational radius of a bead was measured from a major radius of the ellipsoid in the $X-Y$ plot. Conversion voltage to displacement was calibrated by using a piezo-electric stage. All experiments were performed at 25 °C.

### Calculation of the generated torque

The generated torque of the motor ($M$) was calculated from its rotational frictional drag coefficient ($f_r$) multiplied by the angular velocity (ω), $M = f_r \times \omega$. $f_r$ was estimated from the sum of the rotational frictional drag coefficient resulting from the rotation of the bead ($f_b$) and the flagellar filament ($f_f$). $f_b$ and $f_f$ were calculated as:[38,39]

$$f_b = 8\pi\eta r_b^3 + 6\pi\eta r_b r_r^2$$

$$f_f = 2\pi L r^2 (2p^2 + 4\pi^2 r^2)\eta / \{(p^2 + 4\pi^2 r^2)(\ln(2p/d) - 0.5)\}$$

Here, $r_b$ is the radius of a bead, $r_r$ is the rotational

radius of a bead, $L = 5.02$ µm is the length of a filament, $d = 0.016$ µm is the radius of a filament, $r = 0.14$ µm is the helical radius, $p = 1.58$ µm is the helical pitch. $L$, $d$, $r$ and $p$ of *V. alginolyticus* are values measured with TEM.[37] $\eta = 9.6 \times 10^{-4}$ Pa s is the viscosity of the motility medium.

## Acknowledgements

## References

1. Berg, H. C. & Anderson, R. A. (1973). Bacteria swim by rotating their flagellar filaments. *Nature*, **245**, 380–382.
2. Manson, M. D., Tedesco, P., Berg, H. C., Harold, F. M. & van der Drift, C. (1977). A protonmotive force drives bacterial flagella. *Proc. Natl Acad. Sci. USA*, **74**, 3060–3064.
3. Matsuura, S., Shioi, J. & Imae, Y. (1977). Motility in *Bacillus subtilis* driven by an artificial protonmotive force. *FEBS Letters*, **82**, 187–190.
4. Hirota, N., Kitada, M. & Imae, Y. (1981). Flagellar motors of alkalophilic *Bacillus* are powered by an electrochemical potential gradient of Na$^+$. *FEBS Letters*, **132**, 278–280.
5. Macnab, R. M. (1996). Flagella and motility. In *Escherichia coli* and *Salmonella* (Neidhardt, F. C., ed.), pp. 123–145, American Society for Microbiology, Washington, DC.
6. Blair, D. F. (1995). How bacteria sense and swim. *Annu. Rev. Microbiol.* **49**, 489–522.
7. Lloyd, S. A., Tang, H., Wang, X., Billings, S. & Blair, D. F. (1996). Torque generation in the flagellar motor of *Escherichia coli*: evidence of a direct role for FliG but not for FliM or FliN. *J. Bacteriol.* **178**, 223–231.
8. Francis, N. R., Sosinsky, G. E., Thomas, D. & Derosier, D. J. (1994). Isolation, characterization and structure of bacterial flagellar motors containing the switch complex. *J. Mol. Biol.* **235**, 1261–1270.
9. Block, S. M. & Berg, H. C. (1984). Successive incorporation of force-generating units in the bacterial rotary motor. *Nature*, **309**, 470–472.
10. Blair, D. F. & Berg, H. C. (1988). Restoration of torque in defective flagellar motors. *Science*, **242**, 1678–1681.
11. Lloyd, S. A. & Blair, D. F. (1997). Charged residues of the rotor protein FliG essential for torque generation in the flagellar motor of *Escherichia coli*. *J. Mol. Biol.* **266**, 733–744.
12. Zhou, J. D. & Blair, D. F. (1997). Residues of the cytoplasmic domain of MotA essential for torque generation in the bacterial flagellar motor. *J. Mol. Biol.* **273**, 428–439.

13. Zhou, J. D., Lloyd, S. A. & Blair, D. F. (1998). Electrostatic interactions between rotor and stator in the bacterial flagellar motor. *Proc. Natl Acad. Sci. USA*, **95**, 6436–6441.
14. Yorimitsu, T., Sowa, Y., Ishijima, A., Yakushi, T. & Homma, M. (2002). The systematic substitutions around the conserved charged residues of the cytoplasmic loop of Na$^+$-driven flagellar motor component PomA. *J. Mol. Biol.* **320**, 403–413.
15. McCarter, L. L. (2001). Polar flagellar motility of the *Vibrionaceae*. *Microbiol. Mol. Biol. Rev.* **65**, 445–462.
16. Yorimitsu, T. & Homma, M. (2001). Na$^+$-driven flagellar motor of *Vibrio*. *Biochim. Biophys. Acta*, **1505**, 82–93.
17. Okunishi, I., Kawagishi, I. & Homma, M. (1996). Cloning and characterization of *motY*, a gene coding for a component of the sodium-driven flagellar motor in *Vibrio alginolyticus*. *J. Bacteriol.* **178**, 2409–2415.
18. Okabe, M., Yakushi, T., Kojima, M. & Homma, M. (2002). MotX and MotY, specific components of the sodium-driven flagellar motor, colocalize to the outer membrane in *Vibrio alginolyticus*. *Mol. Microbiol.* **46**, 125–134.
19. Okabe, M., Yakushi, T., Asai, Y. & Homma, M. (2001). Cloning and characterization of *motX*, a *Vibrio alginolyticus* sodium-driven flagellar motor gene. *J. Biochem.* **130**, 879–884.
20. Asai, Y., Kawagishi, I., Sockett, E. & Homma, M. (1999). Hybrid motor with the H$^+$- and Na$^+$-driven components can rotate *Vibrio* polar flagella by using sodium ions. *J. Bacteriol.* **181**, 6322–6338.
21. Caplan, S. R. & Karaivanov, M. (1993). The bacterial flagellar motor. *Int. Rev. Cytol.* **147**, 97–164.
22. Berry, R. M. & Armitage, J. P. (1999). The bacterial flagella motor. *Advan. Microb. Physiol.* **41**, 291–337.
23. Silverman, M. & Simon, M. I. (1974). Flagellar rotation and the mechanism of bacterial motility. *Nature*, **249**, 73–74.
24. Lowe, G., Meister, M. & Berg, H. C. (1987). Rapid rotation of flagellar bundles in swimming bacteria. *Nature*, **325**, 637–640.
25. Washizu, M., Kurahashi, Y., Iochi, H., Kurosawa, O., Aizawa, S., Kudo, S. *et al.* (1993). Dielectrophoretic measurement of bacterial motor characteristics. *IEEE Trans. Ind. Appl.* **29**, 286–294.
26. Berg, H. C. & Turner, L. (1993). Torque generated by the flagellar motor of *Escherichia coli*. *Biophys. J.* **65**, 2201–2216.
27. Kudo, S., Magariyama, Y. & Aizawa, S.-I. (1990). Abrupt changes in flagellar rotation observed by laser dark-field microscopy. *Nature*, **346**, 677–680.
28. Kamimura, S. (1987). Direct measurement of nanometric displacement under an optical microscope. *Appl. Optics*, **26**, 3425–3427.
29. Svoboda, K., Schmidt, C. F., Schnapp, B. J. & Block, S. M. (1993). Direct observation of kinesin stepping by optical trapping interferometry. *Nature*, **365**, 721–727.
30. Finer, J. T., Simmons, R. M. & Spudich, J. A. (1994). Single myosin molecule mechanics: piconewton forces and nanometre steps. *Nature*, **368**, 113–119.
31. Ishijima, A., Kojima, H., Funatsu, T., Tokunaga, M., Higuchi, H., Tanaka, H. & Yanagida, T. (1998). Simultaneous observation of individual ATPase and mechanical events by a single myosin molecule during interaction with actin. *Cell*, **92**, 161–171.

32. Ryu, W. S., Berry, R. M. & Berg, H. C. (2000). Torque-generating units of the flagellar motor of *Escherichia coli* have a high duty ratio. *Nature*, **403**, 444–447.

33. Chen, X. & Berg, H. C. (2000). Torque–speed relationship of the flagellar rotary motor of *Escherichia coli*. *Biophys. J.* **78**, 1036–1041.

34. Kojima, S., Atsumi, T., Muramoto, K., Kudo, S., Kawagishi, I. & Homma, M. (1997). *Vibrio alginolyticus* mutants resistant to phenamil, a specific inhibitor of the sodium-driven flagellar motor. *J. Mol. Biol.* **265**, 310–318.

35. Follett, E. A. C. & Gordon, J. (1963). An electron microscope study of *Vibrio* flagellar. *J. Gen. Microbiol.* **32**, 235–239.

36. Kamimura, S. & Kamiya, R. (1992). High-frequency vibration in flagellar axonemes with amplitudes reflecting the size of tubulin. *J. Cell Biol.* **116**, 1443–1454.

37. Magariyama, Y., Sugiyama, S., Muramoto, K., Kawagishi, I., Imae, Y. & Kudo, S. (1995). Simultaneous measurement of bacterial flagellar rotation rate and swimming speed. *Biophys. J.* **69**, 2154–2162.

38. Muramoto, K., Kawagishi, I., Kudo, S., Magariyama, Y., Imae, Y. & Homma, M. (1995). High-speed rotation and speed stability of sodium-driven flagellar motor in *Vibrio alginolyticus*. *J. Mol. Biol.* **251**, 50–58.

39. Berg, H. C. (1993). *Random Walks in Biology*, Princeton University Press, Princeton, NJ.

40. Oosawa, F. & Hayashi, S. (1983). Coupling between flagellar motor rotation and proton flux in bacteria. *J. Phys. Soc. Jpn*, **52**, 4019–4028.

41. Läuger, P. (1988). Torque and rotation rate of the bacterial flagellar motor. *Biophys. J.* **53**, 53–65.

42. Meister, M., Caplan, S. R. & Berg, H. C. (1989). Dynamics of a tightly coupled mechanism for flagellar rotation. *Biophys. J.* **55**, 905–914.

43. Berry, R. M. (1993). Torque and switching in the bacterial flagellar motor. An electrostatic model. *Biophys. J.* **64**, 961–973.

44. Berry, R. M. & Berg, H. C. (1999). Torque generated by the flagellar motor of *Escherichia coli* while driven backward. *Biophys. J.* **31**, 580–587.

45. Atsumi, T. (2001). An ultrasonic motor model for bacterial flagellar motors. *J. Theor. Biol.* **213**, 31–51.

46. Iwazawa, J., Imae, Y. & Kobayasi, S. (1993). Study of the torque of the bacterial flagellar motor using a rotating electric field. *Biophys. J.* **64**, 925–933.

47. Berry, R. M. & Berg, H. C. (1997). Absence of a barrier to backwards rotation of the bacterial flagellar motor demonstrated with optical tweezers. *Proc. Natl Acad. Sci. USA*, **94**, 14433–14437.

48. Muramoto, K., Sugiyama, S., Cragoe, E. J. & Imae, Y. (1994). Successive inactivation of the force-generating units of sodium-driven bacterial flagellar motors by a photoreactive amiloride analog. *J. Biol. Chem.* **269**, 3374–3380.

49. Chen, X. & Berg, H. C. (2000). Solvent-isotope and pH effects on flagellar rotation in *Escherichia coli*. *Biophys. J.* **78**, 2280–2284.

50. Harold, F. M. & Maloney, P. C. (1996). Energy transduction by ion currents. In *Escherichia coli* and *Salmonella* (Neidhardt, F. C., ed.), pp. 283–306, American Society for Microbiology, Washington, DC.

51. Hirota, N. & Imae, Y. (1983). Na$^+$-driven flagellar motors of an alkalophilic *Bacillus* strain YN-1. *J. Biol. Chem.* **258**, 10577–10581.

52. Liu, J. Z., Dapice, M. & Khan, S. (1990). Ion selectivity of the *Vibrio alginolyticus* flagellar motor. *J. Bacteriol.* **172**, 55236–55244.

53. Manson, M. D., Tedesco, P. & Berg, H. C. (1980). Energetics of flagellar rotation in bacteria. *J. Mol. Biol.* **138**, 541–561.

54. Yoshida, S., Sugiyama, S., Hojo, Y., Tokuda, H. & Imae, Y. (1990). Intracellular Na$^+$ kinetically interferes with the rotation of the Na$^+$-driven flagellar motors of *Vibrio alginolyticus*. *J. Biol. Chem.* **256**, 20346–20350.

55. Meister, M., Lowe, G. & Berg, H. C. (1987). The proton flux through the bacterial flagellar motor. *Cell*, **49**, 643–650.

56. Minamino, T., Imae, Y., Oosawa, F., Kobayashi, Y. & Oosawa, K. (2003). Effect of intracellular pH on rotational speed of bacterial flagellar motors. *J. Bacteriol.* **185**, 1190–1194.

57. Yanagida, T., Harada, Y. & Ishijima, A. (1993). Nanomanipulation of actomyosin molecular motors in vitro: a new working principle. *Trends Biochem. Sci.* **18**, 319–324.